Effects of cyclic loading on the mechanical properties and failure of human patellar tendon

Colin R. Firminger[1,2,3], W. Brent Edwards[1,2,3]

[1]Human Performance Laboratory, Faculty of Kinesiology, University of Calgary, Canada

[2]Biomedical Engineering Graduate Program, University of Calgary, Canada

[3]McCaig Institute for Bone and Joint Health, University of Calgary, Canada

Corresponding Author: Colin Firminger

Mailing Address: KNB 219, Human Performance Laboratory, University of Calgary, 2500 University Drive NW, Calgary, AB Canada, T2N 1N4

Phone: 403-808-2601

Email: cfirming@ucalgary.ca

Word Count: 3734

Keywords: Fatigue loading; Tendinopathy; Digital image correlation; Tendon mechanics; Surface strain distributions

Abstract

Patellar tendinopathy is a common overuse injury in sports such as volleyball, basketball, and long-distance running. Microdamage accumulation, in response to repetitive loading of the tendon, plays an important role in the pathophysiology of patellar tendinopathy. This damage presents mechanically as a reduction in Young's modulus and an increase in residual strain. In this study, 19 human patellar tendon samples underwent cyclic testing in load control until failure, segmented by four ramped tests where digital image correlation (DIC) was used to assess anterior surface strain distributions. Ramped tests were performed prior to cyclic testing and at timepoints corresponding to 10%, 20%, and 30% of cyclic stiffness reduction. Young's modulus significantly decreased and cyclic energy dissipation significantly increased over the course of cyclic testing. The DIC analysis illustrated a heterogeneous strain distribution, with strain concentrations increasing in magnitude and size over the course of cyclic testing. Peak stress and initial peak strain magnitudes significantly correlated with the number of cycles to failure (r^2=0.65 and r^2=0.57, respectively, $p<0.001$); however, the rates of peak cyclic strain and modulus loss displayed the highest correlations with the number of cycles to failure (r^2=96% and r^2=86%, respectively, $p<0.001$). The high correlation between the rates of peak cyclic strain and modulus loss suggest that non-invasive methods to continuously monitor tendon strain may provide meaningful predictions of overuse injury in the patellar tendon.

Introduction

Patellar tendinopathy is a common overuse injury observed in athletes participating in sports characterized by repetitive loading and cumulative bouts of activity (Cook et al., 1997; Ferretti et al., 1984; Lian, 2005; Malliaras et al., 2015). Patellar tendinopathy has an insidious onset and a prolonged recovery time, forcing many athletes to retire early from sport (Cook et al., 1997; Kettunen et al., 2002; Malliaras et al., 2015). Tendinopathy is associated with degenerative changes including collagen disorganization, hypercellularity, and hypervascularization (Kannus and Jozsa, 1991; Tallon et al., 2001), as well as reduced Young's modulus (Arya and Kulig, 2010). The pathophysiology of tendinopathy remains a strong topic of debate (Millar et al., 2017), but whether a purely mechanically or biologically mediated phenomenon, tendon damage associated with repetitive loading plays a decided role in this injury (Fung et al., 2010).

The effects of fatigue loading have been observed at several length scales within the extracellular matrix, including collagen molecule denaturation (Zitnay et al., 2020), fibril sliding (Lee and Elliott, 2019), kinked fibers (Szczesny et al., 2018), and complete matrix disruptions (Fung et al., 2010; Gibbon et al., 1999; Nakama et al., 2005). The degradation of collagen in response to fatigue loading causes material property deterioration in the form of reduced tissue modulus and ultimate tensile strength, along with increased cyclic energy dissipation and peak cyclic strain. (Fung et al., 2010; Schechtman and Bader, 2002; Wren et al., 2003). While the exact relationship between microdamage accumulation and tissue mechanical properties is complex, quantifying the effects of cyclic loading on tendon mechanical properties may be used to predict the fatigue failure of tendon.

The influence of cyclic loading on the fatigue behaviour of tendon has been examined in several animal models (Fung et al., 2010; Ker et al., 2000; Pike et al., 2000; Thorpe et al., 2015; Wang et al., 1995); however, research examining human tendon is limited (Schechtman and Bader, 2002, 1997; Wren et al., 2003). Previous studies of human tendon performed *in vitro* cyclic tests of cadaveric extensor digitorum longus (Schechtman and Bader, 2002, 1997) and Achilles (Wren et al., 2003**)** tendons, reporting significant exponential relationships between fatigue life (i.e., the number of cycles to failure) and both peak stress and initial peak strain. While these venerable studies highlighted the important relationship between peak stress/strain magnitude and the fatigue life of tendon, specific details of this relationship are likely to differ amongst different anatomical locations, as the fatigue quality of tendon appears to be highly adapted to the stresses experienced during daily activity (Ker et al., 2000; Pike et al., 2000).

Previous studies utilizing optical methods to track tendon displacement at the tissue level illustrated that tissue strains are location-dependent (Wren et al., 2003). Digital image correlation (DIC) is a state-of-the-art technique that has been used to non-invasively quantify strains across the entire surface of a material by tracking the displacement of a stochastic speckle pattern (Luyckx et al., 2014; Palanca et al., 2016). By integrating this technique into a fatigue test, spatiotemporal changes in strain can be visualized, potentially providing insight into the failure mechanism for tendons under cyclic loading.

Understanding how cyclic loading alters the material properties of human patellar tendon may be used to identify pertinent metrics that are associated with fatigue failure and create tools to monitor the risk of developing patellar tendinopathy. Therefore, the purpose of this study was to quantify

the fatigue behaviour of human patellar tendon using nominal and DIC-based measures. More specifically, we sought to evaluate changes in tissue modulus, cyclic energy dissipation, and DIC-based anterior surface strains during cyclic loading, and to establish correlations between fatigue life with measures of stress, strain, and time-dependent measures such as the rate of peak cyclic strain increase (i.e., creep rate) and Young's modulus degradation rate (i.e., damage rate). We hypothesized cyclic loading would decrease tissue modulus and increase cyclic energy dissipation and surface strains over the course of the fatigue test, and that fatigue life would be well described by non-linear relationships with stress, strain, creep rate, and damage rate.

Methods

Specimen Preparation and Test Setup

Thirty fresh-frozen cadaveric knees (mid-thigh to mid-shank) were obtained from Science Care (AZ, USA). Cadaveric testing was approved by the University of Calgary's Conjoint Health Research Ethics Board (REB18-0970). Prior to dissection, specimens were thawed for 12 hours in a plastic bag submerged in lukewarm water followed by computed tomography (CT) imaging (Revolution HD GSI; GE Healthcare, IL, USA) to examine for any obvious joint pathology. Scans were performed with a peak voltage of 120 kVp, a tube current of 220 mA, with an in-plane resolution = 0.39 × 0.39 mm and a slice thickness of 0.63 mm. Next, the patellar tendon (attached to the patella and tibia) was dissected stored in a -20°C freezer for a maximum of 6 months.

Prior to mechanical testing, each specimen was thawed for 45 minutes at room temperature while fully submerged in saline. A handheld reciprocating bone saw (M.SR-SCT; Foredom, CT, USA) was then used to cut the tibial diaphysis 40 mm inferior to the patellar tendon enthesis and to

remove the tibial plateau (Figure 1a). The medial, lateral, and posterior aspects of the tibia between the cut and the patellar tendon enthesis were removed to create a rectangular shape that could be held in a vertical clamp without touching the patellar tendon enthesis. The medial and lateral portions of the patellar tendon were removed by cutting parallel to the tendon fascicles with a scalpel (Figure 1a). This was necessary to reduce the force required to produce a given tendon stress, as pilot testing identified that the bony endpoints occasionally fractured at high loading magnitudes.

The patellar tendons were inverted and placed into two custom made clamps (Figure 1b) with both entheses outside of the clamped region. The lower clamp was rotated to create a patella-patellar tendon angle of 146° (180° = straight), corresponding to the average knee angle at peak tendon strain during a maximal countermovement jump (Firminger et al., 2019; Schmid et al., 2002). A laser level (DW088K; Dewalt , MD, USA) was used to ensure the tendon was vertical, and a matte black acrylic speckle pattern was painted on to the tendon's anterior surface using an airbrush with a 0.3 mm tip (Master Precision G444; Master Airbrush, China). Gauge length was measured with digital calipers as the distance between the patellar and tibial entheses. Cross-sectional area was calculated assuming a rectangular cross-section as this best represented the tendon geometry following the preparation protocol. Cross-sectional area was measured using digital calipers by averaging the results from three width and three thickness measurements taken halfway along the gauge length.

Mechanical Testing

Tendon samples were cyclically loaded until failure (i.e., full tendon rupture), segmented by four ramped loading tests to capture images for DIC analysis (Figure 2). An ElectroPuls E10000 materials testing machine was used for all mechanical tests (Instron, MS, USA). Samples were kept moist using four saline drips positioned on the tendon, each with a flow rate of 0.2 $mL \cdot min^{-1}$. The selected flow rate was selected based on pilot testing, and ensured that the sample was visibly hydrated throughout the testing procedure (i.e., excess saline was dripping from the tendon).

Cyclic testing was performed in load control using a 2 Hz sinusoidal waveform. The tendons were loaded between 2 MPa and a randomly assigned peak stress, ranging between 11% and 60% of the estimated 60 MPa ultimate tensile strength (UTS) for patellar tendon (Hashemi et al., 2005; Johnson et al., 1994; Noyes et al., 1984). This range of stress values was selected to span estimated patellar tendon loads during walking and jogging (Firminger and Edwards, 2016; Lee and Hidler, 2008). Data were captured at 200 Hz for every cycle until the 100^{th} cycle, then every 10^{th} cycle until the 1000^{th} cycle, and for every 100^{th} cycle thereafter. Maximum and minimum force and displacement were captured for every cycle. The system's compliance was measured using a custom aluminum part held between the upper and lower clamps that was loaded at 100 $N \cdot s^{-1}$ to 2000 N. Displacements of the cyclic loading tests were then corrected by subtracting the system's compliance.

The first ramped loading test was performed prior to the cyclic testing protocol and consisted of a preload test of 5 cycles with a 1 Hz sinusoidal waveform between 0 and 2 MPa, followed by a ramped load from 0 MPa to the tendon-specific peak stress at a rate of 100 $N \cdot s^{-1}$. During the

ramped load, an AVE2 non-contacting video extensometer (Instron, MS, USA) captured images of the anterior patellar tendon surface at a rate of 50 Hz. The images were 542 mm × 80 mm in size and had a resolution of 0.26 mm/pixel. Subsequent ramped loading tests were performed after stiffness (calculated between 30% and 75% of the peak stress of the loading curve for each cycle) decreased by 10%, 20%, and 30% of the maximum cyclic stiffness. In these instances, the cyclic test was paused, the ramped loading test was completed, and the cyclic test was restarted immediately.

Cyclic Test Data Processing

Force data were divided by cross sectional area to calculate stress, and displacement data were converted to nominal strain by dividing displacement (corrected for compliance) by the sample gauge length. Cyclic stress-strain curves were created for every 10% of fatigue life (N_f). The 50th cycle was used for 0% N_f as this allowed the patella and tibia to seat properly within the clamps. Young's modulus was calculated at each percentage of N_f as the slope between 50% and 100% of peak force. Cyclic energy dissipation, calculated as the difference between the area under the loading and unloading stress-strain curves, was numerically computed using the trapezoidal method. A damage parameter was also used to calculate the damage rate per cycle (Cotton et al., 2005):

$$D_i = 1 - \frac{E_i}{E_0} \quad (1)$$

where E_i is the Young's modulus for a given cycle and E_0 is the initial Young's modulus. Damage rate was calculated as the slope of the damage versus loading cycles curve between 30% and 70% of N_f, as this corresponded to the linear portion of the curve (Figure 5f). Creep rate was calculated

as the slope of the peak cyclic strain versus loading cycles, also between 30% and 70% of N_f (Figure 5e).

DIC Processing

Commercially available software (DIC Replay; Instron, MS, USA) was used to calculate axial strains from the video extensometer images. Briefly, a region of interest containing the patellar and tibial entheses was created around the tendon, and a 31 × 31 pixel subset size was used to calculate the displacement of the speckle pattern. The software automatically overlapped neighboring subsets to create a displacement grid spacing equal to one quarter of the subset size. An axial strain colourmap was generated automatically from the displacement grid, which was filtered using a 9 × 9 pixel filter. Custom Matlab code (version R2017b; MathWorks, MA, USA) was used to extract axial strain at peak stress for all pixels within the colourmap based on their greyscale value. Initial median and 99^{th} percentile axial strains were calculated using the strain distributions from the ramped loading tests. Using the DIC software, a virtual extensometer was placed at the patellar and tibial entheses to obtain an overall measure of initial peak tendon strain (referred to as initial nominal strain).

Statistical Analysis

Repeated measures ANOVAs were used to compare Young's modulus and cyclic energy dissipation for every 10% of N_f. A Huynh-Feldt correction was used if the assumption of sphericity was violated, and Bonferroni post hoc tests were performed to examine pairwise differences when a significant main effect was observed. Stress, initial nominal strain, initial median strain, initial 99^{th} percentile strain, creep rate, and damage rate were plotted against N_f to assess the relationship

between these variables and the fatigue behaviour of the patellar tendon. All statistical analyses were performed using SPSS (version 26; IBM, NY, USA) with a criterion alpha-level of 0.05.

Results

A total of 11 samples failed by fracture of the patella or tibia, and it was interesting to note these samples came from donors that weighed less and had lower bone mineral content, as was later confirmed using a quantitative CT mineral analysis of the proximal tibia (Edwards et al., 2013). (Table 1). Of the 19 samples that were successfully tested, 5 had to be re-clamped because some slippage of the bony endpoints in the clamps was observed. These samples were excluded from the analysis of creep rate and damage rate. The exact failure location in the successful samples could not be identified, as fascicles began to progressively fail at an increasing rate until the tendon could not sustain the applied force and ruptured completely. However, we observed that the fascicles tended to rupture near both the patellar and tibial entheses.

A significant effect of cyclic loading was observed for Young's modulus ($F(2.47, 1) = 101.86$, $p < 0.001$; see Figure 3). Post hoc tests revealed that Young's modulus increased significantly between 0% and 10% N_f ($p = 0.010$), followed by significant decreases from 40% to 50% N_f ($p = 0.029$), 70% to 80% N_f ($p < 0.001$), 80% to 90% N_f ($p < 0.001$) and 90% N_f to failure ($p < 0.001$). A significant but less pronounced effect of cyclic loading was also observed for cyclic energy dissipation ($F(1.03,1) = 11.914$, $p = 0.003$; see Figure 3). Post hoc tests demonstrated significant increases in energy dissipation between 0% and 10% N_f ($p = 0.020$) and between 80% and 90% N_f ($p = 0.022$).

Relationships between N_f and the outcome variables of stress, strain, creep rate and damage rate were quantified using power law relationships (Figure 5), as these generally displayed better fits than exponential relationships. Peak stress explained 65% of the variance in N_f ($p < 0.001$), and both initial peak nominal strain and initial median strain displayed significant relationships with N_f ($r^2 = 0.57$ and $r^2 = 0.60$, respectively, $p < 0.001$ for both). However, initial 99th percentile strain did not correlate well with N_f ($r^2 = 0.07$, $p = 0.265$). Creep rate had the strongest relationship with N_f, explaining 96% of the variance in N_f ($p < 0.001$), followed by damage rate, which explained 86% of the variance in N_f ($p < 0.001$).

DIC strain distributions visualized at 90%, 80% and 70% of the maximum cyclic stiffness consistently showed increased axial strains near the tendon entheses. Strain concentrations were also present within the tendon midsubstance and tended to increase in size and magnitude throughout the test (see Figure 6).

Discussion

The purpose of this study was to quantify the fatigue behaviour and associated material property degradation of human patellar tendon. We observed significant decreases in Young's modulus and increases in cyclic energy dissipation over the course of the cyclic test. Fatigue life was well described by power law relationships for initial nominal strain, initial median strain, and peak stress, but creep rate and damage rate were by far the best predictors. Strain concentrations, calculated using DIC, increased in both size and magnitude over the course of cyclic testing. These data provide important information for our understanding of patellar tendon overuse injuries.

We observed an increase in Young's modulus at the beginning of cyclic testing, followed by a steady decrease between 30% and 70% N_f, with a sharper decrease from 70% N_f until failure. Expectedly, an opposite trend was observed for cyclic energy dissipation, which initially decreased from 0-10% N_f, and then stabilized until 80% N_f when it sharply increased until failure. These findings indicate that in a fatigue loading scenario, the patellar tendon may be able to sustain a threshold level of energy dissipation until failure is imminent, while tendon stiffness continues to decrease until failure. The observed reductions in Young's modulus and increases in energy dissipation with cyclic loading may be attributed to microdamage accumulation (Fung et al., 2010, 2009), which originates from the denaturation of collagen molecules (Zitnay et al., 2020).

Microdamage accumulation in tendon is indeed strain controlled (Fung et al., 2010; Schechtman and Bader, 1997; Wren et al., 2001; Zitnay et al., 2020), therefore we expected measures of initial strain to be highly correlated with fatigue-life measurements. We discovered that the amount of variance described by the relationship between peak initial strain and the fatigue life of the patellar tendon (r^2 = 57%) was similar to that of the Achilles tendon (r^2 = 59%) from the work of Wren et al. (2003). However, the slope of our power law fit was 4.3, which is considerably less than the slope of 9.3 for the Achilles tendon (Figure 7). While it is tempting to suggest that the fatigue life of Achilles tendon is more sensitive to changes in initial strain than the patellar tendon, it is important to note that fatigue-life measurements from Wren et al., (2003) corresponded to low cycle fatigue (between 10^0-10^4 cycles) and displayed more scatter than the patellar tendon results presented herein. Combining the Achilles and patellar tendon data together increased the amount of explained variance substantially (r^2 = 78%, Figure 7), and visual inspection supports the notion that these two tendons illustrate similar fatigue behaviour.

Human tendon has been observed to rupture at a relatively homogenous peak strain magnitude between 13% and 20% in both monotonic and cyclic testing scenarios (Butler et al., 1986; Cooper et al., 1993; Hashemi et al., 2005; Johnson et al., 1994; Schechtman and Bader, 1997; Wren et al., 2001). Thus, one would expect measures that account for the cyclic- or time-dependent increases in peak strain to be highly correlated with fatigue-life measurements. In this study, the creep rate explained 96% of the variance in fatigue life, which interestingly, is identical to the amount of variance explained by creep rate for human cortical bone samples loaded in cyclic uniaxial tension (Cotton et al., 2005). These findings have important implications for the prediction of overuse injuries in biological tissues. For tendon, if changes to peak cyclic strain over time could be tracked using non-invasive measures (through ultrasound or some other means), this may prove much more valuable than relying on initial estimates of peak stress or strain obtained through biomechanical analysis, for example (Firminger et al., 2020).

As expected, DIC surface strains increased as the tendon accumulated fatigue damage. We also observed localized areas of increased strain (Figure 6) which did not extend the entire length of the tendon, supporting the notion that load was likely being delivered via shear stress across discontinuous fibrils (Svensson et al., 2013; Szczesny et al., 2015; Szczesny and Elliott, 2014). The heterogeneity of strains across the tendon surface indicates that fatigue damage did not accrue equally across the entire tendon. Rather, weaker areas illustrated increases in strain magnitude and strain concentration size as the tendon stiffness degraded.

Patellar tendinopathy is considered to be an “insertional tendinopathy” as the symptomatic region is generally located at or near the patellar enthesis. Interestingly, most samples in our study failed near the patellar and tibial entheses. While these observations may be associated with anterior surface strain concentrations which were commonly observed near the entheses, previous research has speculated that patellar tendinopathy may occur due to shear stresses caused by disparities in strain magnitude between the anterior and posterior surfaces near the patellar enthesis (Maganaris et al., 2004). As we were only able to quantify anterior surface strains, future work examining posterior surface strains using a similar protocol may be able to further elucidate the mechanisms of failure near the patellar enthesis.

Despite decreasing the cross-sectional area of the patellar tendon to avoid specimen pull-out or bone fracture prior to tendon failure, 11 samples fractured pre-emptively at the patella or tibia. Though not an *a priori* objective of this study, we were able to determine that these samples had lower bone mass by analyzing CT images that were originally captured to remove potential specimens with obvious joint pathology. Because the samples that successfully completed the cyclic tests had higher bone mass metrics, we postulated that bone and tendon quality may be correlated in some way. Thus, in a post hoc analysis, we plotted integral measures of bone mineral content (BMC), bone volume (BV), and bone mineral density (BMD) against tendon fatigue life to see whether any relationships existed. None of the aforementioned measures of integral bone mass correlated with fatigue life (BMC, $r^2 = 0.002$; BV, $r^2 = 0.082$; BMD, $r^2 = 0.018$), suggesting that measure of bone mass are not strong surrogate markers of tendon quality.

The findings from this study are limited to *in vitro* mechanical fatigue tests of cadaveric specimens. The damage state of tendon *in vivo* will, of course, depend on biological repair and adaptation processes, although it is worth noting that tendon may have limited ability for repair (Heinemeier and Kjaer, 2011; Langberg et al., 1999; Miller et al., 2005). Another important limitation of this study is that we were unable to test the full cross-sectional area of the patellar tendon as some of the patella and tibia specimens were likely too weak to withstand the necessary forces required to hold them in the clamp. We acknowledge that removing the medial and lateral portions of the tendon may have altered the tendon's native fatigue properties. However, we were careful to not damage the remaining tendon fascicles and kept a large enough amount of tendon to consider the structure as a subset of the original structure.

Conclusions

Patellar tendon samples illustrated decreased stiffness and increased energy dissipation over the course of cyclic testing. Using DIC, we observed the existence of weaker localized strains in areas that grew in size and magnitude as stiffness degraded, illustrating that fatigue damage did not accumulate equally across the entire tendon surface. The fatigue behaviour was well defined by initial nominal strain and initial median strain, further illustrating the strain-dependence of tendon failure in cyclic loading. The excellent correlation between both creep rate and damage rate with fatigue life suggests that non-invasive measurements that track continuous changes in tendon strain may prove effective for preventing overuse injuries of the patellar tendon.

Conflicts of interest

The authors have no competing or financial interests to disclose.

Funding

Research funding was provided in part by the Natural Sciences and Engineering Research Council of Canada (NSERC; RGPIN 01029-2015, CGSD3 504212-2017), Alberta Innovates, and the NBA/GE Healthcare Orthopedics and Sports Medicine Collaboration. Research infrastructure was funded by a Canadian Foundation for Innovation John R. Evans Leaders Fund (Project #37134).

References

Arya, S., Kulig, K., 2010. Tendinopathy alters mechanical and material properties of the Achilles tendon. J. Appl. Physiol. 108, 670–5. doi:10.1152/japplphysiol.00259.2009

Butler, D., Kay, M., Stouffer, D., 1986. Comparison of Material Properties in Fascicle-Bone Units From Human Patellar Tendon and Knee Ligaments. J. Biomech. 19, 425–432. doi:https://doi.org/10.1016/0021-9290(86)90019-9

Cook, J.L., Khan, K.M., Harcourt, P.R., Grant, M., Young, D.A., Bonar, S.F., 1997. A cross sectional study of 100 athletes with jumper's knee managed conservatively and surgically. The Victorian Institute of Sport Tendon Study Group. Br. J. Sports Med. 31, 332–336. doi:10.1136/bjsm.31.4.332

Cooper, D., Deng, X.H., Burstein, A.L., Warren, R.F., 1993. The strength of the central third tendon graft. Am. J. Sports Med. 21, 818–824.

Cotton, J.R., Winwood, K., Zioupos, P., Taylor, M., 2005. Damage rate is a predictor of fatigue life and creep strain rate in tensile fatigue of human cortical bone samples. J. Biomech. Eng. 127, 213–219. doi:10.1115/1.1865188

Edwards, W.B., Schnitzer, T.J., Troy, K.L., 2013. Torsional stiffness and strength of the proximal tibia are better predicted by finite element models than DXA or QCT. J. Biomech. 46, 1655–1662. doi:10.1016/j.jbiomech.2013.04.016

Ferretti, A., Puddu, G., Mariani, P.P., Neri, M., 1984. Jumper's knee: an epidemiological study of volleyball players. Phys. Sportsmed. 12, 97–106. doi:10.1080/00913847.1984.11701970

Firminger, C.R., Asmussen, M.J., Cigoja, S., Fletcher, J.R., Nigg, B.M., Edwards, W.B., 2020. Cumulative Metrics of Tendon Load and Damage Vary Discordantly with Running Speed. Med. Sci. Sport. Exerc. Publish Ah, 1549–1556. doi:10.1249/mss.0000000000002287

362 Firminger, C.R., Bruce, O.L., Wannop, J.W., Stefanyshyn, D.J., Edwards, W.B., 2019. Effect of
363 Shoe and Surface Stiffness on Lower Limb Tendon Strain in Jumping, Medicine & Science
364 in Sports & Exercise. doi:10.1249/MSS.0000000000002004
365 Firminger, C.R., Edwards, W.B., 2016. The influence of minimalist footwear and stride length
366 reduction on lower-extremity running mechanics and cumulative loading. J. Sci. Med. Sport
367 19, 975–979. doi:10.1016/j.jsams.2016.03.003
368 Fung, D.T., Wang, V.M., Andarawis-Puri, N., Basta-Pljakic, J., Li, Y., Laudier, D.M., Sun, H.B.,
369 Jepsen, K.J., Schaffler, M.B., Flatow, E.L., 2010. Early response to tendon fatigue damage
370 accumulation in a novel in vivo model. J. Biomech. 43, 274–279.
371 doi:10.1016/j.jbiomech.2009.08.039
372 Fung, D.T., Wang, V.M., Laudier, D.M., Shine, J.H., Basta-Pljakic, J., Jepsen, K.J., Schaffler,
373 M.B., Flatow, E.L., 2009. Subrupture tendon fatigue damage. J. Orthop. Res. 27, 264–273.
374 doi:10.1002/jor.20722
375 Gibbon, W.W., Cooper, J.R., Radcliffe, G.S., 1999. Sonographic incidence of tendon microtears
376 in athletes with chronic Achilles tendinosis. Br. J. Sports Med. 33, 129–130.
377 doi:10.1136/bjsm.33.2.129
378 Hashemi, J., Chandrashekar, N., Slauterbeck, J., 2005. The mechanical properties of the human
379 patellar tendon are correlated to its mass density and are independent of sex. Clin. Biomech.
380 20, 645–652. doi:10.1016/j.clinbiomech.2005.02.008
381 Heinemeier, K.M., Kjaer, M., 2011. In vivo investigation of tendon responses to mechanical
382 loading. J. Musculoskelet. Neuronal Interact. 11, 115–123.
383 Johnson, G.A., Tramaglini, D.M., Levine, R.E., Ohno, K., Choi, N.Y., Woo, S.L.Y., 1994.
384 Tensile and viscoelastic properties of human patellar tendon. J. Orthop. Res. 12, 796–803.

doi:10.1002/jor.1100120607

Kannus, P., Jozsa, L., 1991. Histopathological changes preceding spontaneous rupture of a tendon. J. Bone Jt. Surg. 73-A, 1507–1525.

Ker, R.F., Wang, X.T., Pike, A.V.L., 2000. Fatigue quality of mammalian tendons. J. Exp. Biol. 203, 1317–27. doi:10.2165/00007256-199520020-00003

Kettunen, J.A., Kvist, M., Alanen, E., Kujala, U.M., 2002. Long-Term Prognosis for Jumper's Knee in Male Athletes. Am. J. Sports Med. 30, 689–692. doi:10.1177/03635465020300051001

Langberg, H., Skovgaard, D., Petersen, L.J., Bülow, J., Kjaer, M., 1999. Type I collagen synthesis and degradation in peritendinous tissue after exercies determined by microdialysis in humans. J. Physiol. 521, 299–306.

Lee, A.H., Elliott, D.M., 2019. Multi-Scale Loading and Damage Mechanisms of Plantaris and Rat Tail Tendons. J. Orthop. Res. 37, 1827–1837. doi:10.1002/jor.24309

Lee, S.J., Hidler, J., 2008. Biomechanics of overground vs. treadmill walking in healthy individuals. J. Appl. Physiol. 104, 747–755. doi:10.1152/japplphysiol.01380.2006

Lian, O.B., 2005. Prevalence of Jumper's Knee Among Elite Athletes From Different Sports: A Cross-sectional Study. Am. J. Sports Med. 33, 561–567. doi:10.1177/0363546504270454

Luyckx, T., Verstraete, M., De Roo, K., De Waele, W., Bellemans, J., Victor, J., 2014. Digital image correlation as a tool for three-dimensional strain analysis in human tendon tissue. J. Exp. Orthop. 1, 7. doi:10.1186/s40634-014-0007-8

Maganaris, C.N., Narici, M. V, Almekinders, L.C., Maffulli, N., 2004. Biomechanics and Pathophysiology of Overuse Tendon Injuries Ideas on Insertional Tendinopathy 34, 1005–1017.

Malliaras, P., Cook, J., Purdam, C., Rio, E., 2015. Patellar tendinopathy: Clinical diagnosis, load management, and advice for challenging case presentations. J. Orthop. Sports Phys. Ther. 45, 887–898. doi:10.2519/jospt.2015.5987

Millar, N.L., Murrell, G.A.C., Mcinnes, I.B., 2017. Inflammatory mechanisms in tendinopathy - towards translation. Nat. Rev. Rheumatol. 13, 110–122. doi:10.1038/nrrheum.2016.213

Miller, B.F., Olesen, J.L., Hansen, M., Døssing, S., Crameri, R.M., Welling, R.J., Langberg, H., Flyvbjerg, A., Kjaer, M., Babraj, J.A., Smith, K., Rennie, M.J., 2005. Coordinated collagen and muscle protein synthesis in human patella tendon and quadriceps muscle after exercise. J. Physiol. 567, 1021–1033. doi:10.1113/jphysiol.2005.093690

Nakama, L.H., King, K.B., Abrahamsson, S., Rempel, D.M., 2005. Evidence of tendon microtears due to cyclical loading in an in vivo tendinopathy model. J. Orthop. Res. 23, 1199–1205. doi:10.1016/j.orthres.2005.03.006

Noyes, F.R., Butler, D.L., Grood, E.S., Zernicke, R.F., Hefzy, M.S., 1984. Biomechanical Analysis of Human Knee Ligament Grafts used in Knee Ligament Repairs and Reconstructions. J Bone Jt. Surg AM 66, 344–352.

Palanca, M., Tozzi, G., Cristofolini, L., 2016. The use of digital image correlation in the biomechanical area: A review. Int. Biomech. 3, 1–21. doi:10.1080/23335432.2015.1117395

Pike, A.V.L., Ker, R.F., Alexander, R.M., 2000. The development of fatigue quality in high- and low-stressed tendons of sheep (Ovis aries). J. Exp. Biol. 203, 2187–2193.

Schechtman, H., Bader, D.L., 2002. Fatigue damage of human tendons. J. Biomech. 35, 347–353.

Schechtman, H., Bader, D.L., 1997. In vitro fatigue of human tendons. J. Biomech. 30, 829–835.

Schmid, M., Hodler, J., Cathrein, P., Duewell, S., Jacob, H., Romero, J., 2002. Is impingement

the cause of jumper's knee? Dynamic and static magnetic resonance imaging of patellar tendinitis in an open-configuration system. Am. J. Sports Med. 30, 388–395. doi:10.1177/03635465020300031401

Svensson, R.B., Mulder, H., Kovanen, V., Magnusson, S.P., 2013. Fracture mechanics of collagen fibrils: Influence of natural cross-links. Biophys. J. 104, 2476–2484. doi:10.1016/j.bpj.2013.04.033

Szczesny, S.E., Aeppli, C., David, A., Mauck, R.L., 2018. Fatigue loading of tendon results in collagen kinking and denaturation but does not change local tissue mechanics. J. Biomech. 71, 251–256. doi:10.1016/j.jbiomech.2018.02.014

Szczesny, S.E., Caplan, J.L., Pedersen, P., Elliott, D.M., 2015. Quantification of interfibrillar shear stress in aligned soft collagenous tissues via notch tension testing. Sci. Rep. 5, 1–9. doi:10.1038/srep14649

Szczesny, S.E., Elliott, D.M., 2014. Interfibrillar shear stress is the loading mechanism of collagen fibrils in tendon. Acta Biomater. 10, 2582–2590. doi:10.1016/j.actbio.2014.01.032

Tallon, C., Maffulli, N., Ewen, S.W.B., 2001. Ruptured Achilles tendons are significantly more degenerated than tendinopathic tendons. Med. Sci. Sports Exerc. 33, 1983–1990. doi:10.1097/00005768-200112000-00002

Thorpe, C.T., Chaudhry, S., Lei, I.I., Varone, A., Riley, G.P., Birch, H.L., Clegg, P.D., Screen, H.R.C., 2015. Tendon overload results in alterations in cell shape and increased markers of inflammation and matrix degradation. Scand. J. Med. Sci. Sport. 25, e381–e391. doi:10.1111/sms.12333

Wang, X.T., Ker, R.F., Alexander, R.M., 1995. Fatigue rupture of wallaby tail tendons. J. Exp. Biol. 198, 847–852.

Wren, T.A.L., Lindsey, D.P., Beaupre, G.S., Carter, D.R., 2003. Effects of creep and cyclic loading on the mechanical properties and failure of human Achilles tendons. Ann. Biomed. Eng. 31, 710–717. doi:10.1114/1.1569267

Wren, T.A.L., Yerby, S.A., Beaupré, G.S., Carter, D.R., 2001. Mechanical properties of the human achilles tendon. Clin. Biomech. 16, 245–251. doi:10.1016/S0268-0033(00)00089-9

Zitnay, J.L., Jung, G.S., Lin, A.H., Qin, Z., Li, Y., Yu, S.M., Buehler, M.J., Weiss, J.A., 2020. Accumulation of collagen molecular unfolding is the mechanism of cyclic fatigue damage and failure in collagenous tissues. Sci. Adv. 6.

Tables

Table 1: Summary of donor information and indices of tibial integral bone mineral

Test Result	Age (years)	Height (cm)	Weight (kg)	BMI (kg/m^2)	Sex (male/female)	BV (cm^3)	BMC (g)	BMD (g/cm^3)
Successful	73.6 (12.7)	172.5 (8.9)	77.3 (15.6)	25.9 (4.4)	14/5	192.41 (46.36)	45.04 (18.14)	0.23 (0.09)
Unsuccessful	80.8 (12.8)	168.3 (9.2)	66.4 (9.0)	24.7 (3.7)	5/6	162.08 (36.21)	28.42 (21.49)	0.16 (0.10)
All	76.2 (14.3)	170.9 (9.1)	73.3 (14.4)	25.5 (4.1)	19/11	181.58 (44.83)	39.10 (20.66)	0.21 (0.10)
p-value	0.187	0.244	0.043	0.458	-	0.086	0.039	0.063

Independent samples t-tests were performed to assess statistical differences between successful and unsuccessful tests.

Figures

Figure 1: a) Schematic of sample preparation; the tibia was transected 40 mm distal to the tibial tuberosity and was machined to fit into the upper clamp. The proximal 10 mm of the tibia was also removed to allow for adequate spacing between the tibia and the lower clamp. b) Experimental setup of the fatigue test. The prepared sample was inverted, with the tibia held in the upper clamp and the patella held in the lower clamp at an angle of 146° to the patellar tendon. Four saline drips kept the sample hydrated during testing.

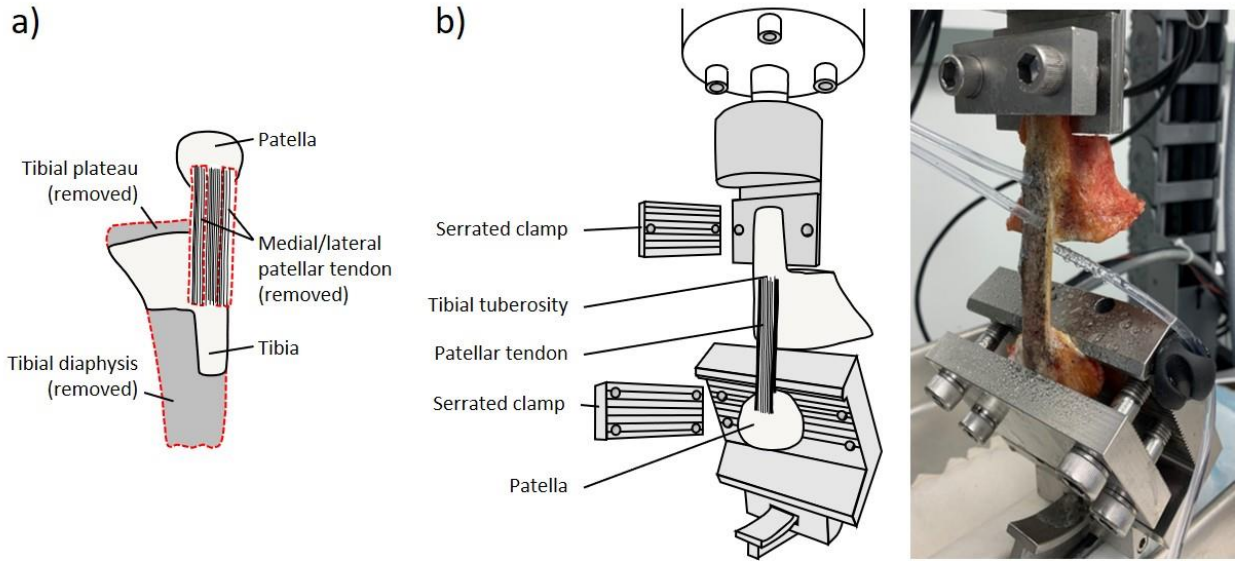

Figure 2: Stiffness profile of a representative sample cyclically loaded between 2 MPa and the test stress at 2 Hz until failure (red X). Ramped tests with DIC were performed prior to cyclic loading, and at 90%, 80% and 70% of maximum cyclic stiffness (k_{max}).

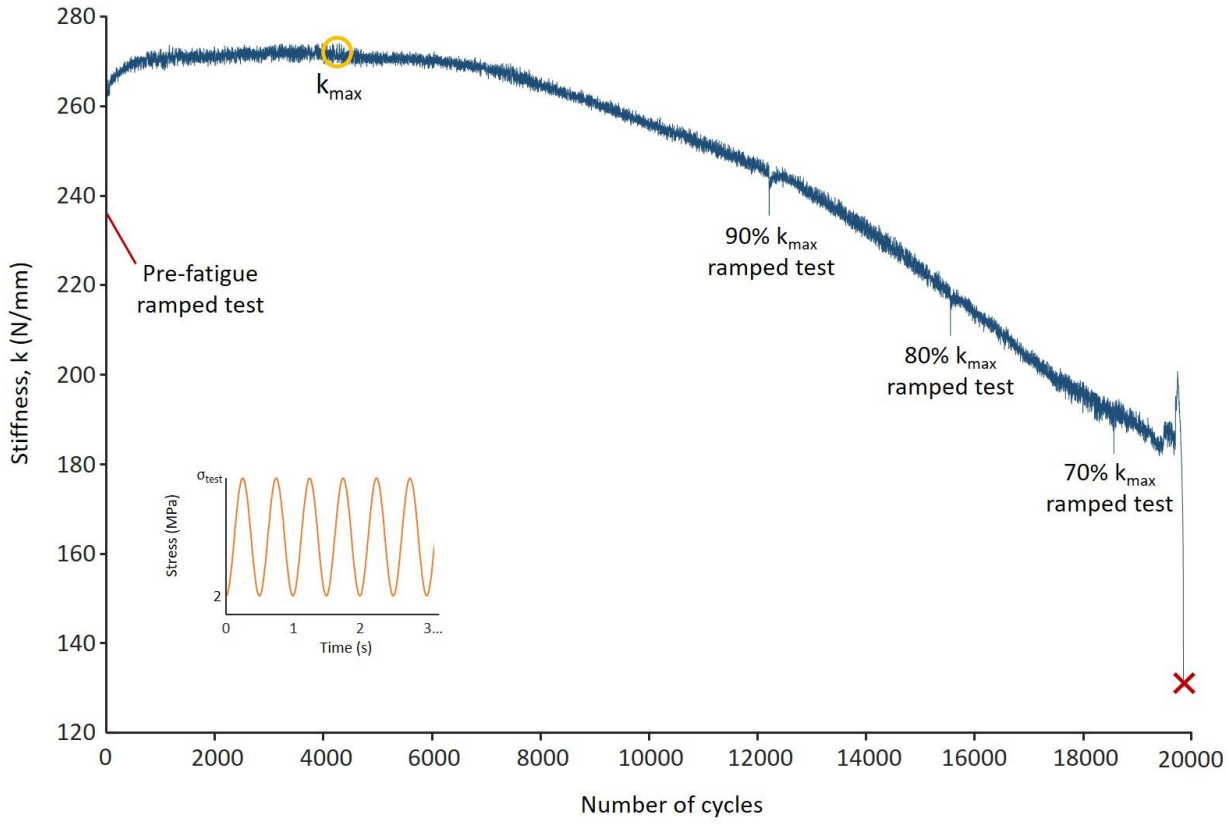

Figure 3: Stress-strain cycles 0-100% fatigue life (N_f) for a representative sample.

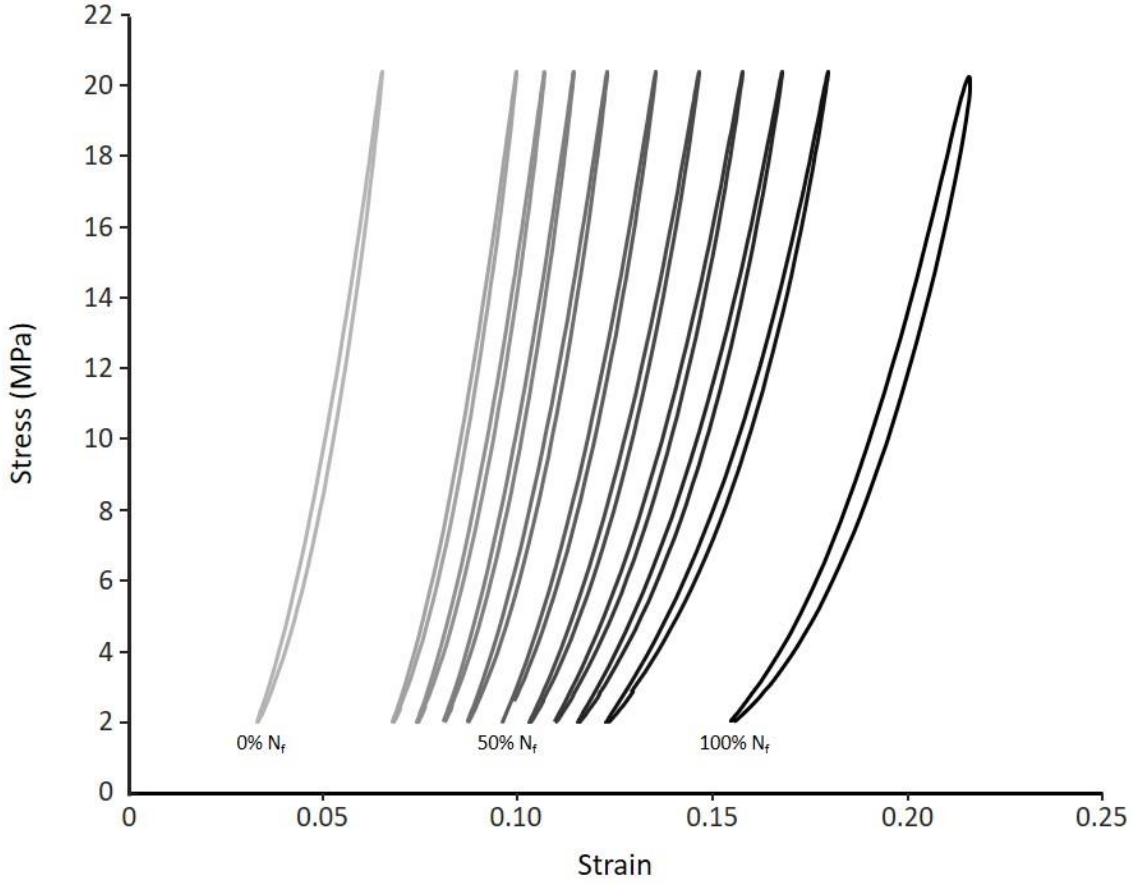

Figure 4: Estimated marginal means ± standard deviation for: a) Young's modulus and b) energy dissipation of stress-strain cycles from 0-100% fatigue life (N_f). *Significant difference ($p < 0.05$).

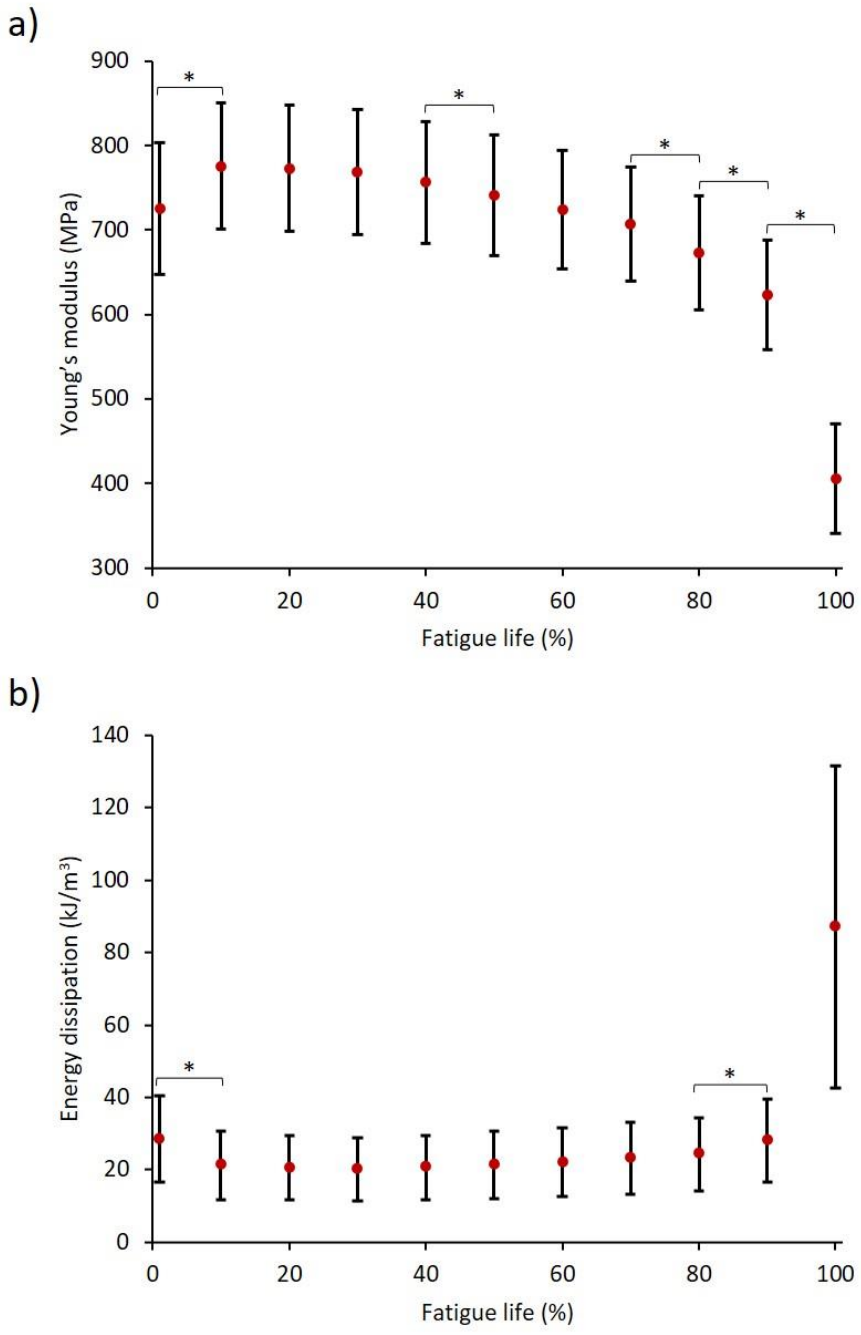

Figure 5: Plots of a) peak stress, b) initial peak nominal strain, c) initial median strain, d) initial 99th percentile strain, e) creep rate, and f) damage rate, versus fatigue life. All plots have been fitted with a power law curve. The insets in e) and f) illustrate how creep rate and damage rate were calculated using a representative sample.

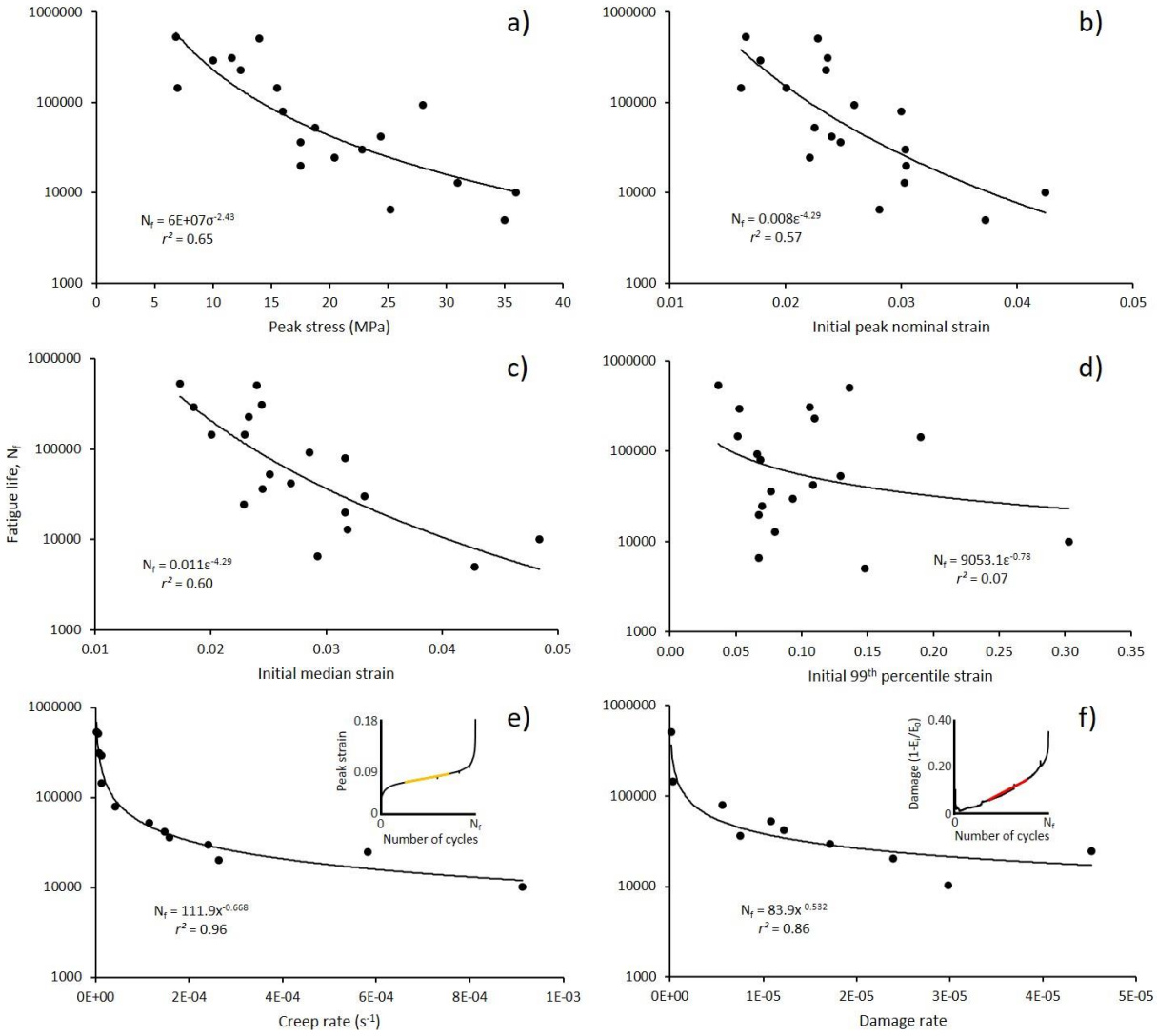

Figure 6: Axial surface strains of a representative sample: a) prior to the fatigue test; b) at 90% of the maximum cyclic stiffness; c) at 80% of the maximum cyclic stiffness; d) at 70% of the maximum cyclic stiffness.

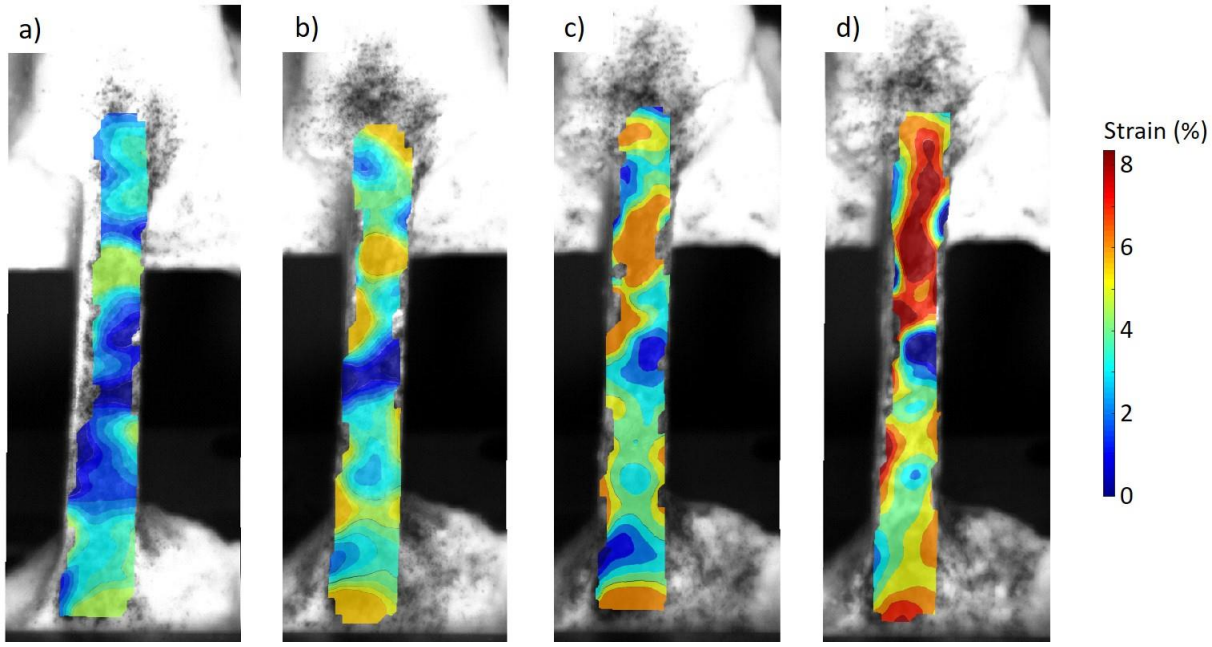

Figure 7: Initial nominal strain versus fatigue life for the patellar and Achilles tendons (red and blue points, respectively). Achilles tendon data were obtained from Wren et al (2003). Individual power law curves fitted to patellar ($N_{f,\,PT}$) and Achilles ($N_{f,\,AT}$) tendon data illustrated similar amounts of explained variance. Pooling the patellar and Achilles tendon data ($N_{f,\,Both}$) explained a larger amount of variance than the individual curves.